JACS
JOURNAL OF THE AMERICAN CHEMICAL SOCIETY
Article
pubs.acs.org/JACS

Cooperative Effect of Monopodal Silica-Supported Niobium Complex Pairs Enhancing Catalytic Cyclic Carbonate Production

Valerio D'Elia,[†,§] Hailin Dong,[†,§] Aaron J. Rossini,[‡] Cory M. Widdifield,[‡] Sai V. C. Vummaleti,[†] Yury Minenkov,[†] Albert Poater,[†,⊥] Edy Abou-Hamad,[†] Jérémie D. A. Pelletier,*[,†] Luigi Cavallo,[†] Lyndon Emsley,[∥,‡] and Jean-Marie Basset*[,†]

[†]KAUST Catalysis Center, King Abdullah University of Science and Technology, Thuwal 23955-6900, Saudi Arabia

[‡]Centre de RMN à Très Hauts Champs (CNRS/ENS-Lyon/UCB Lyon 1), Université de Lyon, 5 rue de la Doua, 69100 Villeurbanne, France

[⊥]Institut de Química Computacional, Department de Química, Universitat de Girona, Campus de Montilivi, E-17071 Girona, Spain

[∥]Institut des Sciences et Ingénierie Chimiques, Ecole Polytechnique Fédérale de Lausanne (EPFL), CH-1015 Lausanne, Switzerland

Supporting Information

ABSTRACT: Recent discoveries highlighted the activity and the intriguing mechanistic features of $NbCl_5$ as a molecular catalyst for the cycloaddition of CO_2 and epoxides under ambient conditions. This has inspired the preparation of novel silica-supported Nb species by reacting a molecular niobium precursor, $[NbCl_5{\cdot}OEt_2]$, with silica dehydroxylated at 700 °C ($SiO_{2\text{-}700}$) or at 200 °C ($SiO_{2\text{-}200}$) to generate diverse surface complexes. The product of the reaction between $SiO_{2\text{-}700}$ and $[NbCl_5{\cdot}OEt_2]$ was identified as a monopodal supported surface species, $[{\equiv}SiONbCl_4{\cdot}OEt_2]$ (**1a**). The reactions of $SiO_{2\text{-}200}$ with the niobium precursor, according to two different protocols, generated surface complexes **2a** and **3a**, presenting significant, but different, populations of the monopodal surface complex along with bipodal $[({\equiv}SiO)_2NbCl_3{\cdot}OEt_2]$. ^{93}Nb solid-state NMR spectra of **1a**−**3a** and ^{31}P solid-state NMR on their PMe_3 derivatives **1b**−**3b** led to the unambiguous assignment of **1a** as a single-site monopodal Nb species, while **2a** and **3a** were found to present two distinct surface-supported components, with **2a** being mostly monopodal $[{\equiv}SiONbCl_4{\cdot}OEt_2]$ and **3a** being mostly bipodal $[({\equiv}SiO)_2NbCl_3{\cdot}OEt_2]$. A double-quantum/single-quantum ^{31}P NMR correlation experiment carried out on **2b** supported the existence of vicinal Nb centers on the silica surface for this species. **1a**−**3a** were active heterogeneous catalysts for the synthesis of propylene carbonate from CO_2 and propylene oxide under mild catalytic conditions; the performance of **2a** was found to significantly surpass that of **1a** and **3a**. With the support of a systematic DFT study carried out on model silica surfaces, the observed differences in catalytic efficiency were correlated with an unprecedented cooperative effect between two neighboring Nb centers on the surface of **2a**. This is in an excellent agreement with our previous discoveries regarding the mechanism of $NbCl_5$-catalyzed cycloaddition in the homogeneous phase.

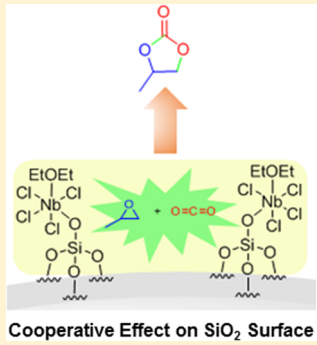

INTRODUCTION

Niobium coordination compounds are well known in Lewis acid catalysis.[1] We recently disclosed $NbCl_5$ as an excellent catalyst for the cycloaddition of CO_2 and epoxides under ambient conditions in the presence of organic nucleophiles as co-catalysts.[2] Further kinetic and theoretical studies on the reaction mechanism suggested a bimetallic step of CO_2 activation. Accordingly, the barrier for the insertion of CO_2 in the sterically crowded Nb−O bond formed after epoxide ring-opening is strongly reduced by the interaction of CO_2 with a second Nb center.[3] It was therefore of high interest to explore the mechanism of the process by using supported Nb species. Through surface organometallic chemistry (SOMC) methodologies, we were able to produce, with an excellent degree of control, diverse typologies of silica-supported Nb coordination compounds such as isolated monopodal Nb species, bipodal species, and neighboring Nb complexes, that constituted an ideal toolset to study the mechanism on the surface.

Niobium complexes supported on metal oxide surfaces have not yet been explored in SOMC or coordination chemistry on surfaces. This lack of reports can be explained by the relative experimental difficulty, compared to other early metal counterparts (i.e., zirconium,[4] titanium,[4] tantalum,[5] tungsten[6]), in preparing and handling niobium alkyl complexes.[7] Nevertheless, using coordination compounds without alkyl ligands is difficult because they are rarely monomeric and usually generate a diversity of surface sites upon grafting. Furthermore, the characterization of such species is also complicated by the absence of hydrocarbon fragments coordinated to the metal, thus hindering the application of typical solid-state (SS) NMR techniques (i.e., ^{1}H and ^{13}C SSNMR).[4,8] In this context, several recent studies have been directed toward gaining structural insight into the grafting sites by a more direct observation of

Received: March 19, 2015
Published: May 7, 2015

DOI: 10.1021/jacs.5b02872
J. Am. Chem. Soc. 2015, 137, 7728−7739

the surface complexes. Indeed, the oxygen atoms linked to the metal can be observed by ^{17}O SSNMR.[9] The NMR-active nuclei such as ^{27}Al[10] and ^{51}V[11] of grafted metal complexes or the ligand atoms ($^{35/37}Cl$)[12] can also be probed via SSNMR experiments. Niobium-93 nuclei are NMR active but have never been used as probes to observe surface species. ^{93}Nb SSNMR experiments have been reported on niobium-containing organometallics and on niobium-based materials such as niobia and niobium-doped derivatives.[13] To our knowledge, there are no examples of well-defined silica-supported surface Nb derivatives, nor of their systematic characterization and application in catalysis.

We report a new and simple strategy to graft niobium pentachloride on a silica surface, in which varying the dehydroxylation temperature of the support and the amount of Nb precursor employed resulted in different types of surface compounds that have been extensively characterized by FT-IR and by ^{1}H, ^{13}C, and ^{93}Nb solid-state multinuclear magnetic resonance experiments. These surface species were used as heterogeneous catalysts for the cycloaddition of CO_2 to propylene oxide (PO) to form propylene carbonate in the presence of NBu_4Br as a source of bromide ions. The study confirms the importance of the cooperative interaction between two Nb atoms in the mechanism of the reaction and shows an unprecedented degree of interaction between surface-supported species.

RESULTS AND DISCUSSION

Surface niobium compounds **1a**, **2a**, and **3a** were prepared by treatment of silica dehydroxylated at 700 °C ($SiO_{2\text{-}700}$) or at 200 °C ($SiO_{2\text{-}200}$) with niobium pentachloride dissolved in diethyl ether in defined stoichiometric proportions with the expected number of surface silanols (Scheme 1 and Table 1).

Scheme 1. Proposed Main Surface Component Structures and Preparative Conditions for the Niobium Surface Compounds 1a−3a Grafted on $SiO_{2\text{-}700}$ (1a) and on $SiO_{2\text{-}200}$ (2a, 3a) Using $NbCl_5{\cdot}OEt_2$ as a Molecular Precursor[a]

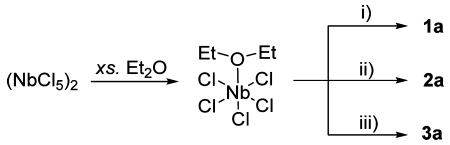

[a]Conditions: (i) $SiO_{2\text{-}700}$ (1 g), $NbCl_5{\cdot}OEt_2$ (0.91 equiv of SiOH/mmol Nb), Et_2O, rt, 3 h; (ii) $SiO_{2\text{-}200}$ (1 g), $NbCl_5{\cdot}OEt_2$ (0.75 equiv of SiOH/mmol Nb), Et_2O, rt, 20 h; (iii) $SiO_{2\text{-}200}$ (1 g), $NbCl_5{\cdot}OEt_2$ (1.50 equiv of SiOH/mmol Nb), Et_2O, rt, 20 h. See also Table 1.

Table 1. Elemental Analysis of 1a−3a

	$NbCl_5{\cdot}OEt_2$[a]	SiOH[b] (equiv)	grafted Nb[c]	Nb/SiOH	Cl[d,f] (equiv)	C[e] (equiv)
1a	0.33	0.30 (0.91)	0.30	1.0	1.01 (3.4)	1.41 (4.7)
2a	1.04	0.78 (0.75)	0.65	0.83	2.00 (3.1)	2.41 (3.7)
3a	0.52	0.78 (1.50)	0.47	0.60	1.26 (2.7)	1.55 (3.3)

[a]mmol of $NbCl_5{\cdot}OEt_2$ employed per gram of silica. [b]mmol of silanol per gram of silica (SiOH/Nb). [c]mmol of Nb grafted per gram of silica. [d]mmol of chlorine per gram of silica (Cl/Nb). [e]mmol of carbon per gram of silica (C/Nb). [f]Chlorine quantification might be underestimated due to thermal degradation.[14]

Grafting of $NbCl_5{\cdot}OEt_2$ on $SiO_{2\text{-}700}$. Niobium pentachloride is known to be dimeric in the solid state, with two bridging (μ^2) chlorine atoms; the corresponding etherate complex has been shown to exist as monomeric $NbCl_5{\cdot}OEt_2$.[1j,15] In our experiment, the latter was generated *in situ* by dissolution of $[NbCl_5]_2$ in diethyl ether prior to grafting (Scheme 1).[16] This solution was added to $SiO_{2\text{-}700}$, and the slurry was stirred for 3 h at room temperature. The resulting yellow powder was washed three times with Et_2O before being collected under high vacuum (10^{-5} mbar) to yield **1a**. Comparison of the IR spectra of **1a** and $SiO_{2\text{-}700}$ shows the complete disappearance of the sharp band at 3747 cm^{-1} (ν(OH)), indicating the consumption of all the isolated silanols of $SiO_{2\text{-}200}$ (Figure 1). New signals can be assigned to

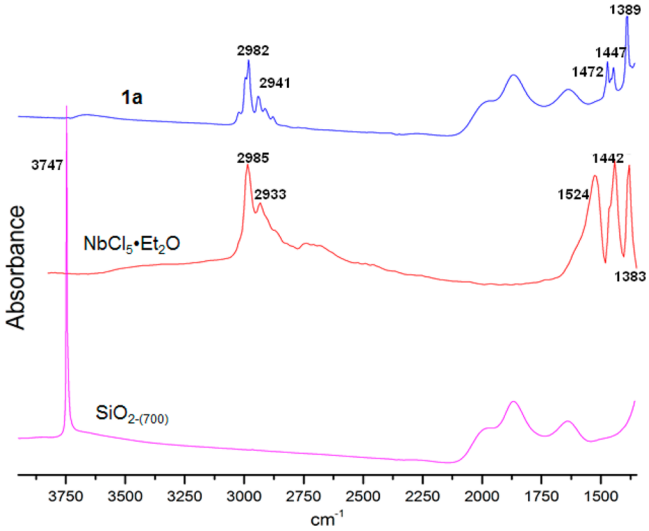

Figure 1. FT-IR spectra of **1a** (blue), $NbCl_5{\cdot}OEt_2$ (red), and $SiO_{2\text{-}700}$ (purple).

the presence of diethyl ether at 2982 and 2941 cm^{-1} (ν_s(C−H)), 1472 and 1447 cm^{-1} (δ_d(H−C−H)), and 1389 cm^{-1} (ν_s(C−O)).[17] The new signals on the $SiO_{2\text{-}200}$ surface are comparable with those displayed in the spectrum of $NbCl_5{\cdot}OEt_2$ (Figure 1). Grafting of the niobium chloride precursor is assumed to proceed through protolysis of the Nb−Cl bond by the surface silanols (liberating gaseous HCl), hence forming at least one Nb−O bond that tethers the complex to the silica surface. The molar amount of niobium supported on silica (Table 1, entry 1) corresponds precisely to the number of silanols available at the surface of $SiO_{2\text{-}700}$ (ca. 3×10^{-4} mol/g of silica).[4] This ratio supports the selective reaction of one silanol with one molecule of $NbCl_5{\cdot}OEt_2$ (Scheme 1). The carbon/niobium molar ratio of 4.72 (theoretical: 4) and the chlorine/niobium molar ratio of 3.37 (theoretical: 4) found for **1a** are in rough agreement with the presence of monopodal niobium complex bound to silica with four chlorides and one diethyl ether ligand. The surface of $SiO_{2\text{-}700}$ is known to exhibit mostly isolated silanols, hence promoting nearly exclusive grafting of monopodal species from contact with metal complexes.[4,9,11] It should be noted that diethyl ether is easily desorbed from the surface of $SiO_{2\text{-}700}$ at ambient temperature when submitted to high vacuum ($<10^{-5}$ mbar). Complementary experiments, grafting $NbCl_5{\cdot}OEt_2$ on $SiO_{2\text{-}700}$ in the absence of solvent (see Supporting Information (SI), Figure S1), revealed the evolution of HCl and validated the protolysis of the Nb−Cl bond via a silanol as the grafting step. Hence, assuming a monopodal niobium tetrachloride surface species bearing one molecule of diethyl

DOI: 10.1021/jacs.5b02872
J. Am. Chem. Soc. 2015, 137, 7728−7739

Scheme 2. Proposed Structures for Silica-Supported Species 1a−3a

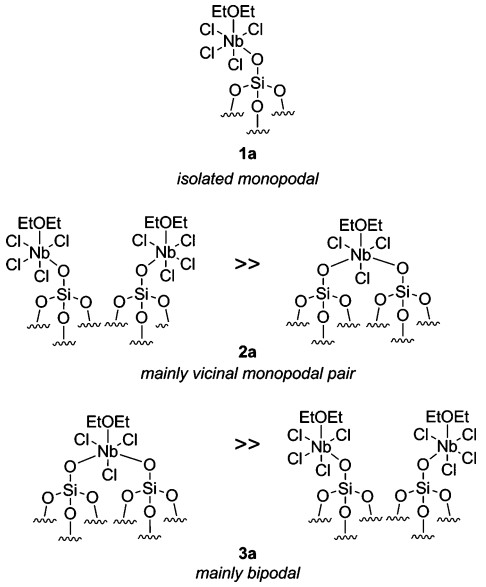

ether, the formula [≡SiONbCl$_4$·OEt$_2$] can be tentatively proposed for **1a** (Scheme 2).

Further understanding of the coordination sphere of the niobium atom was gained by examining the signal of the bound diethyl ether molecule in the IR and SSNMR spectra. Comparison of the ν(C−H) region between 3000 and 2800 cm^{-1} of **1a** and NbCl$_5$·OEt$_2$ (Figure 1) with that of diethyl ether (see SI, Figure S2) reveals a significant difference regarding the pattern of bands between uncoordinated and coordinated ether. Specifically, the spectra of molecular ether, in both the gas and liquid phases, contain two strong signals at 2989 and 2870 cm^{-1}. The latter band, which has been formally assigned to the asymmetric ν_{as}(C−H) stretching of methylene,[17] was not observed in the IR spectrum of either **1a** or NbCl$_5$·OEt$_2$, in which it was replaced by a signal at 2941 or 2933 cm^{-1}, respectively (Figure 1). This may be interpreted as a consequence of the coordination of the diethyl ether to niobium. Unsurprisingly, the proximal methylene group appears to be the most influenced by coordination to the strongly acidic niobium center.[18] The region between 1360 and 1540 cm^{-1} exhibits several differences between NbCl$_5$·OEt$_2$ and Et$_2$O that can be correlated to the methylene vibrations and represent indirect indicators of coordination of ether to NbCl$_5$: noticeably, a broad strong signal at 1524 cm^{-1} (all C−H bending modes are found below 1500 cm^{-1} in uncoordinated ether, Figure S2) and two strong overlapping peaks at 1442 and 1383 cm^{-1}. However, their assignment is complicated because this region also contains vibrations due to the methyl bending bands. Notably, comparable bands are also found in the FT-IR spectrum of **1a**.

The structure of the surface niobium complex **1a** was further investigated by applying ^{1}H MAS and ^{13}C CP/MAS SSNMR to probe the chemical shifts of the coordinating ether molecules (see Figure S3). The resonances due to the terminal methyl were clearly identified at 1.25 ppm (^{1}H MAS) and at 10 ppm (^{13}C CP/MAS) for **1a**. Comparing the chemical shifts of **1a** with those of uncoordinated liquid EtO$_2$, the signals of the methylene groups were significantly shifted downfield: 4.40 vs 3.50 ppm in ^{1}H and 69 vs 65 ppm in ^{13}C (see also Figure S7 for the ^{1}H NMR of uncoordinated ether). In the case of NbCl$_5$·OEt$_2$, the peaks relative to the methylene groups show an even higher downfield shift at 4.68 and 75 ppm in the ^{1}H and ^{13}C NMR, respectively (Figure S3).[18] This may be explained by the replacement of one oxygen atom (e.g., Si−O) by a chlorine in the coordination sphere of the niobium center. All these observations show that diethyl ether can serve as a useful probe for the presence of Lewis acids such as niobium.

Grafting of NbCl$_5$·OEt$_2$: on SiO$_{2\text{-}200}$. Two different grafting protocols were followed, one in which an excess of Nb precursor compared to the expected number of silanols was used (**2a**), and one for which the precursor/SiOH proportions were reversed (**3a**, See Table 1). In the cases of **2a** and **3a**, the FTIR spectra revealed the complete consumption of all isolated silanols at 3747 cm^{-1} and of part of the bridging silanols present on the surface (SiO-H···O(H)Si, broad bands in the 3300−3500 cm^{-1} region, see Figure S4). The new peaks were comparable to those observed for **1a** and were assigned to the formation of niobium etherate complexes. The very broad signals above 3000 cm^{-1} can be attributed to the unconsumed bridging silanols.[15b] Analysis of the ^{1}H MAS and ^{13}C CP/MAS SSNMR spectra of **2a** and **3a** (see Figures S5 and S6) suggests a strong similarity to the NMR spectra of **1a** with a nearly identical pattern of resonances that may be assigned to niobium coordinated diethyl ether. In the cases of **2a**, and **3a**, signals arising from traces of diethyl ether physisorbed onto SiO$_{2\text{-}200}$ can be found in the SSNMR spectra (see Figures S5 and S7). Although some slight differences in the chemical shifts can be observed between the ^{1}H MAS, and ^{13}C CP/MAS SSNMR spectra of **1a**, and **2a** and **3a**, due to the influence of the Nb coordination sphere on the chemical shift at the ^{1}H, and ^{13}C nuclei of the ether ligand, this does not allow the unambiguous distinction between the different surface species. However, according to the elemental analysis data (Table 1), and unlike **1a**, the niobium content found in **2a**, and **3a** (0.65, and 0.47 mmol/g of silica, respectively) is lower than the theoretical metal loading based on the number of silanols present on SiO$_{2\text{-}200}$ (0.78 mmol/g of silica). Considering the density of silanol groups on SiO$_{2\text{-}200}$, the formation of bipodal species on the silica surface can be postulated by substitution of two chlorine atoms on the same NbCl$_5$·OEt$_2$ molecule by vicinal silanols. The amount of niobium in **3a** (0.47 mmol/g of silica) is slightly higher than that previously reported for the bipodal grafting of other transition metals on SiO$_{2\text{-}200}$ (0.38 mmol/g of silica for Zr,[4] 0.42 mmol/g for Ti,[4] 0.42 mmol/g for V[11]) while, in the case of **2a**, higher Nb loading was observed (0.65, vs 0.47 mmol/g). For **2a**, the higher ratio of grafted niobium per silanol (0.83, or roughly one niobium per silanol), suggests that mainly monopodal surface species are formed. The tentative structures for **2a**, and **3a** based on these considerations are reported in Scheme 2. These results show that the density of available silanol groups has a strong influence on the podality of the surface complex formed, with the amount of Nb precursor employed playing an additional role as observed for **2a**. The difference in niobium species density is evident also in the UV−vis diffuse reflectance spectra of **1a−3a** (see Figure S9). In order to further characterize the distinctive properties of the surface species, we studied **1a−3a** using ^{93}Nb SSNMR (*vide infra*) spectroscopy. Reaction of **1a−3a** with a probe molecule trimethylphosphine (PMe$_3$) that completely displaces coordinated ether molecules yielded **1b−3b**. **1b−3b** were studied by ^{31}P SSNMR, as discussed below.

DOI: 10.1021/jacs.5b02872
J. Am. Chem. Soc. 2015, 137, 7728−7739

Probing the Niobium Environment Using Coordinated Trimethylphosphine, and ^{31}P SSNMR Spectroscopy. Surface complexes **1a**−**3a** were contacted with a vapor of PMe_3 to displace the coordinated ether, and enable ^{31}P NMR experiments on the surface species. It is assumed that the phosphine would displace the ether molecule, and remain bound to the surface niobium without being physisorbed or chemisorbed on the surface of the silica. Treatment of $SiO_{2\text{-}700}$ or $SiO_{2\text{-}200}$ by PMe_3 shows that no changes are observed in the ^{1}H, and ^{31}P CP/MAS NMR spectra, and the FTIR spectra of these materials, indicating that the silica surface does not react or retain PMe_3. The resulting complexes **1b**−**3b** were characterized by ^{1}H, and ^{31}P SSNMR (Figure 2). In addition,

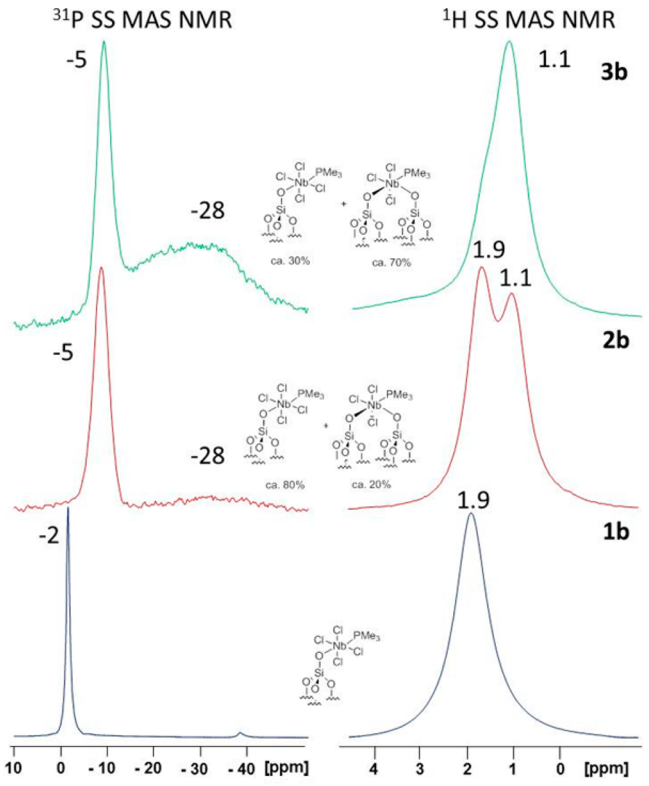

Figure 2. One-dimensional (1D) ^{1}H MAS solid-state NMR spectra of **1b**−**3b** (acquired at 400 MHz with a 10 kHz MAS frequency, a 4 s repetition delay, and 32 scans) and 1D ^{31}P CP/MAS SSNMR spectra of **1b**−**3b** (acquired at 9.4 T, (ν_0(^{1}H) = 400 MHz with a 10 kHz MAS frequency, 5000 scans, 4 s repetition delay, and a 2 ms contact time). Exponential line broadening of 80 Hz was applied prior to Fourier transformation.

2b was subjected to ^{1}H−^{31}P HETCOR and ^{31}P double-quantum/single-quantum NMR experiments (Figures 3 and 4). The ^{1}H MAS and ^{31}P CP/MAS SSNMR spectra of **1b** contain a single peak at 1.9 and −2 ppm, respectively. This set of resonances is consistent with PMe_3 molecules coordinated to a single type of niobium center as expected by treating monopodal **1a** with PMe_3. The spectra of **2b** and **3b** contain, for both nuclei observed, two sets of signals consistent with the existence of a binary mixture of surface complexes differing by the ratio of each component. A narrow peak was found at −5 ppm and a broad peak at −28 ppm in the ^{31}P NMR spectra of both **2b** and **3b**. The former signal indicates phosphorus nuclei with high relative mobility whereas the broad signals are consistent with a far less mobile species. On the basis of such

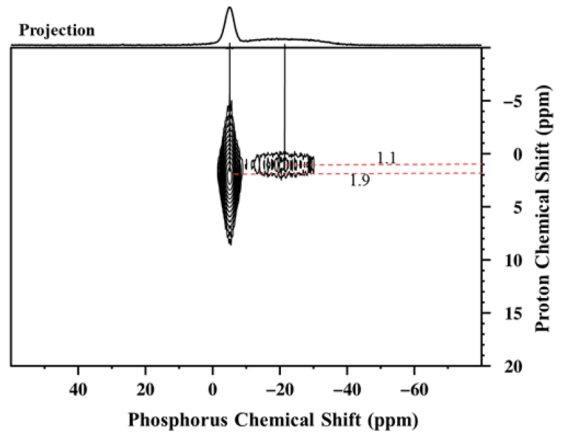

Figure 3. 2D ^{1}H−^{31}P CP/MAS dipolar HETCOR spectrum of **2b** (acquired at 9.4 T with a 10 kHz MAS frequency, 2000 scans per t_1 increment (homonuclear ^{1}H dipolar decoupling was applied during t_1), a 4 s repetition delay, 32 individual t_1 increments, and a 0.2 ms contact time).

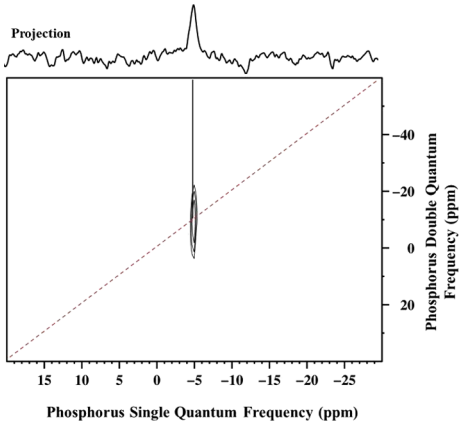

Figure 4. 2D ^{31}P−^{31}P double-quantum (DQ)/single-quantum (SQ) solid-state NMR homonuclear correlation spectrum of **2b**. The spectrum was obtained with the BABA pulse sequence with cross-polarization from ^{1}H.[19] The spectrum was acquired at 9.4 T with a 10 kHz MAS frequency, 8000 scans per t_1 increment, a 4 s repetition delay, 32 individual t_1 increments, and a 2 ms CP contact time.

observations and the high density of SiOH groups on the surface of $SiO_{2\text{-}200}$, it can be tentatively proposed that the peak around −5 ppm is due to PMe_3 coordinated to a monopodal surface niobium atom and that the signal at −28 ppm arises from coordination to its bipodal counterpart. The area of each ^{31}P NMR signal was integrated: **2b** is estimated to contain 80% of monopodal Nb and 20% bipodal Nb, while **3b** is mostly bipodal (70%), with the remaining 30% being monopodal. A similar distribution pattern is observed in the ^{1}H SSNMR spectra with the signals due to the methyl groups of PMe_3 found at 1.9 and 1.1 ppm. A ^{1}H−^{31}P HETCOR spectrum of **2b** (Figure 3) confirms the correlations between resonances at −5 and 1.9 ppm and at −28 and 1.1 ppm, respectively. Moreover, the difference in intensities between these two peaks (1.9 and 1.1 ppm) seems to vary in a consistent manner with the corresponding peaks in the ^{31}P NMR spectra.

Therefore, taken together, the ^{1}H MAS and ^{31}P CP/MAS SSNMR spectra suggest that **1b** contains monopodal species, **2b** contains mainly monopodal species with some bipodal species, and **3b** consists of mainly bipodal species with some

DOI: 10.1021/jacs.5b02872
J. Am. Chem. Soc. 2015, 137, 7728−7739

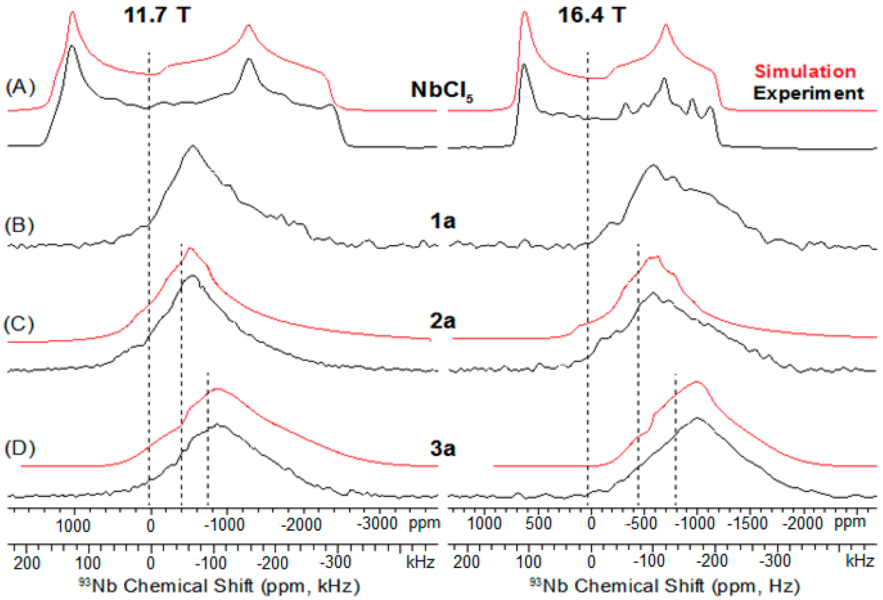

Figure 5. Static ^{93}Nb solid-state NMR spectra acquired at magnetic fields of 11.7 and 16.4 T of (A) $(NbCl_5)_2$, (B) **1a**, (C) **2a**, and (D) **3a**. Analytical simulations of ^{93}Nb NMR powder patterns including chemical shift anisotropy (CSA) and non-coincident electric field gradient (EFG) and CS tensors (indicated by non-zero Euler angles) are shown as red traces above the experimental spectra (black traces). Distributions of the EFG tensor parameters were used for simulations of the spectra of **2a** and **3a**. The extracted EFG tensor parameters and chemical shift tensors are listed in Table S3 in the Supporting Information. The dashed lines indicate the isotropic chemical shift values obtained from the simulations. The spectra and simulations indicate that the isotropic chemical shift of **3a** is reduced by ca. 350 ppm compared to **2a**. Spectra of **1a** were not simulated given the similarity of the spectra to those of **2a**.

monopodal species, in agreement with the structures proposed for **1a**−**3a** in Scheme 2. This assumption is corroborated also by the ^{93}Nb SSNMR spectra of the parent complexes **1a**−**3a** (*vide infra*). Considering that using the same $SiO_{2\text{-}200}$ support leads to either mainly monopodal niobium surface complexes or mainly bipodal complexes, it may be speculated that the monopodal niobium etherate complexes in **2a** are rather close and that they could present neighboring Nb complexes. This is strongly supported by a double-quantum/single-quantum ^{31}P NMR correlation experiment carried out on **2b** (Figure 4) that exhibits a correlation in the −5 ppm single-quantum resonance and confirms that this material presents very close Nb complexes which are potentially in the condition of interacting.

Further information on the relative positions of the niobium phosphorus complexes on the silica surface in **2b** was obtained from a ^{31}P−^{31}P proton driven spin diffusion experiment (Figure S8). The spectrum only shows the presence of autocorrelations even after a long mixing period of 40 ms, suggesting that the phosphorus nuclei in the monopodal and the bipodal surface species are distant from one another and non-interacting.

^{93}Nb Solid-State NMR Spectra of $NbCl_5$ and 1a−3a. The surface species in **1a**−**3a** were further investigated by submitting them to ^{93}Nb SSNMR experiments. Niobium-93 possesses a nuclear spin (I) of 9/2, a moderate gyromagnetic ratio (Larmor frequency, ν_0 = 122 MHz at 11.7 T) and is 100% naturally abundant. The sensitivity of ^{93}Nb is approximately 2870 times that of ^{13}C in natural abundance.[20] ^{93}Nb SSNMR has previously been applied to materials such as oxides,[13e] halides,[21] and organometallic complexes,[13a] for example. In cases where niobium is present in a spherically symmetric coordination environment and thus the quadrupolar coupling constant (C_Q) is small (<50 MHz), the ^{93}Nb NMR powder patterns will typically span tens of kHz in breadth, and magic angle spinning (MAS) can be applied to obtain higher resolution spectra. However, the ^{93}Nb nucleus possesses a moderately large quadrupole moment (Q) of −32 fm^2, which means that ^{93}Nb SSNMR spectra are often severely broadened by the quadrupolar interaction. Some materials yield broad ^{93}Nb spectra because the niobium resides in an environment of low spherical symmetry. In such cases the C_Q is large, and these spectra typically span several hundred kHz.[13e] Hence, MAS cannot be applied to improve resolution, and static wide-line SSNMR techniques are required.[22] Figure 5 shows the static ^{93}Nb SSNMR spectra of $NbCl_5$, **1a**, **2a**, and **3a** acquired with the WURST-QCPMG pulse sequence as it provides uniform broadband excitation and improved sensitivity.[13e] Spectra were acquired at two magnetic fields in order to obtain a more accurate determination of the electric field gradient (EFG) and chemical shift (CS) tensor parameters. Since $NbCl_5$ is crystalline, sharp and distinct features are obtained in its ^{93}Nb NMR powder patterns, and it is straightforward to obtain the EFG and CS tensor parameters, as well as the Euler angles describing the relative orientations of the CS and EFG tensors from analytical simulations (red traces) of the spectra. However, in the cases of **1a**−**3a**, broad and featureless powder patterns are obtained. The broadening of the ^{93}Nb SSNMR spectra and lack of sharp features likely reflect (i) the disordered nature of the amorphous silica surface and (ii) disorder in the position of the coordinating ligands around the niobium center.

Assuming a pseudo-octahedral niobium coordination environment in **1a**−**3a**, it is likely that there is no preference for the ether ligand to reside either "*cis*" or "*trans*" to the silica surface (this is confirmed by DFT calculations on silica models, *vide infra*). DFT calculations using models (see the Experimental Section for information about the model) of a monopodal niobium surface species suggest that the location of the ether

DOI: 10.1021/jacs.5b02872
J. Am. Chem. Soc. 2015, 137, 7728−7739

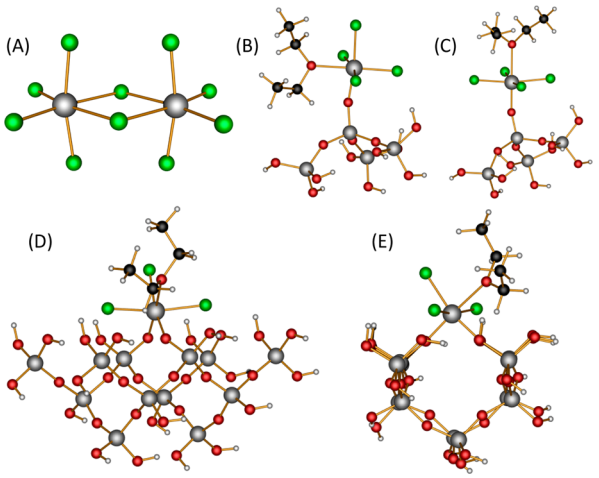

Figure 6. POV-ray renderings of the geometry-optimized structures used to calculate the NMR tensor parameters for $NbCl_5$ (A); monopodal surface species in **1a**/**2a**, where the diethyl ether was placed either "*cis*" (B) or "*trans*" (C) to the model of the $SiO_{2\text{-}700}$ surface; and for the bipodal surface species in **3a** on a model of the $SiO_{2\text{-}200}$ surface (D,E), where two different views have been provided. Color labeling: green, Cl; silver, Nb/Si; black, C; red, O; and white, H. Geometry optimizations and NMR parameter calculations included relativistic effects at the DFT level via the ZORA.

ligand strongly influences the ^{93}Nb EFG tensor parameters (Table S3 and Figure 6). For all of these reasons the ^{93}Nb SSNMR spectra of **2a** and **3a** (given the similarity in the appearance of the spectra of **1a** and **2a**, only the spectra of **2a** were simulated since they were of higher signal-to-noise ratio) were simulated with a distribution of EFG tensor parameters using the QuadFit simulation program (red upper traces).[23] By using a distribution of EFG tensor parameters, it was possible to adequately simulate the broad experimental spectra and obtain the estimated ranges of the EFG tensor, as well as the niobium CS tensor parameters (Table S3). Simulations of the spectra of **2a** and **3a** suggest that the average values of the quadrupolar coupling constants (C_Q) are similar in both cases and are greater than 60 MHz. In both **2a** and **3a**, the average value of the EFG tensor asymmetry parameter (η_Q) was far from zero, suggesting that the EFG tensor parameters is asymmetric, and hence there are no high-order rotational or symmetry axes present for the majority of the surface species. Most importantly, simulations of the spectra of **2a** and **3a** confirm that the isotropic chemical shift (δ_{iso}) of **3a** is about 350 ppm lower than that of **2a**.

DFT Structural Models of 1a−3a and Calculations of ^{93}Nb NMR parameters. In order to better interpret the ^{93}Nb SSNMR spectra, we created structural models of silica-bound monopodal [≡SiONbCl$_4$·OEt$_2$] and of bipodal [(≡SiO)$_2$NbCl$_3$·OEt$_2$] (Figure 6) and subjected them to DFT calculations, to calculate the ^{93}Nb NMR tensor parameters. The DFT calculations predict that large values of C_Q should be obtained for all complexes (except for the *trans* model of **2a**), in agreement with the observation of broad ^{93}Nb NMR spectra for **1a−3a**. The calculations also correctly predict that the niobium nucleus of the surface-supported niobium species should be more shielded (more negative chemical shifts) than those observed for $NbCl_5$. Importantly, the calculations suggest that replacing a chlorine from the Nb coordination sphere with a surface oxide when going from a monopodal tetrachloride to a bipodal trichloride surface species increases the magnetic shielding (decreases the chemical shift) by ca. 200−300 ppm. This is in reasonable accord with the ca. 350 ppm decrease in the niobium chemical shift observed experimentally when comparing the spectra of **2a** (and **1a**) to those of **3a**. Therefore, taken together, the DFT calculations and ^{93}Nb SSNMR spectra indicate that **1a** and **2a** primarily contain monopodal surface species, while **3a** primarily contains bipodal surface species.

These findings are in good agreement with the information obtained from the ^{31}P and ^{1}H SSNMR spectra of **1b−3b**. We have also recently observed via variable temperature ^{13}C SSNMR that grafting of pentamethyl tungsten onto $SiO_{2\text{-}700}$ results in primarily monopodal surface species while grafting onto $SiO_{2\text{-}200}$ results in a substantial fraction (ca. 30%) of bipodal surface species,[24] consistent with the conclusions arrived at by considering the ^{93}Nb SSNMR data for **1a−3a**. Therefore, the combined spectroscopic results show that species **2a** and **3a** differ in the podality of the main surface complex formed during grafting and that this can be attributed to the use of different amounts of $NbCl_5$·OEt_2 during the initial grafting step. This can be rationalized by considering that following the grafting of the first complex, the reaction of a vicinal silanol with a second molecule of $NbCl_5$·OEt_2 to afford neighboring monopodal surface complexes will be in competition with the reaction with the already grafted complex to afford a bipodal surface species. In the cases of **2a** and **3a**, it appears that varying the amount of Nb precursor makes it possible to drive the reaction toward the formation of the desired species as a major component. It remains unclear whether this unusual reactivity is driven by the formation of a loosely coordinated adduct between two Nb complexes before grafting when working at higher precursor concentrations or if it is simply due to the balance of the relative rates of the competing processes. However, DFT calculations on model silica surfaces (*vide infra*) show that in the presence of a grafted [≡SiONbCl$_4$·OEt$_2$] complex both processes (formation of a bipodal species or grafting of a second complex) are thermodynamically favored.

Catalysis. There is renewed interest toward the development of efficient catalytic systems for the synthesis of industrially and synthetically relevant cyclic carbonates from CO_2 and epoxides.[25] We have recently reported simple molecular niobium catalysts and selected organic nucleophiles as efficient homogeneous catalysts for this transformation under ambient conditions.[2] Only a few heterogeneous, recyclable catalysts are able to promote efficiently the cycloaddition of CO_2 and PO under mild conditions: these include one-component, silica-supported bimetallic aluminum salen complexes[26] or MOFs[27] and other microporous organic network systems used in combination with tetralkylammonium salts.[28] In light of the high catalytic activity measured for simple and inexpensive $NbCl_5$ in the homogeneous phase, we tested **1a−3a** for the cycloaddition of CO_2 and PO under mild conditions (60 °C, 10 bar) in the presence of NBu_4Br (tetra-*n*-butylammonium bromide) as a source of bromide ions (see also the SI). All runs selectively yielded propylene carbonate (see Table S1).

Comparison of the conversion data obtained in the first catalytic run shows a strong dependency of the catalytic efficiency on the precatalyst employed; **2a** (90%) surpasses significantly **3a** (61%) and **1a** (25%) (Figure 7). To clearly assess the performance of the surface species, a second run was conducted using the solid phase collected after the initial

DOI: 10.1021/jacs.5b02872
J. Am. Chem. Soc. 2015, 137, 7728−7739

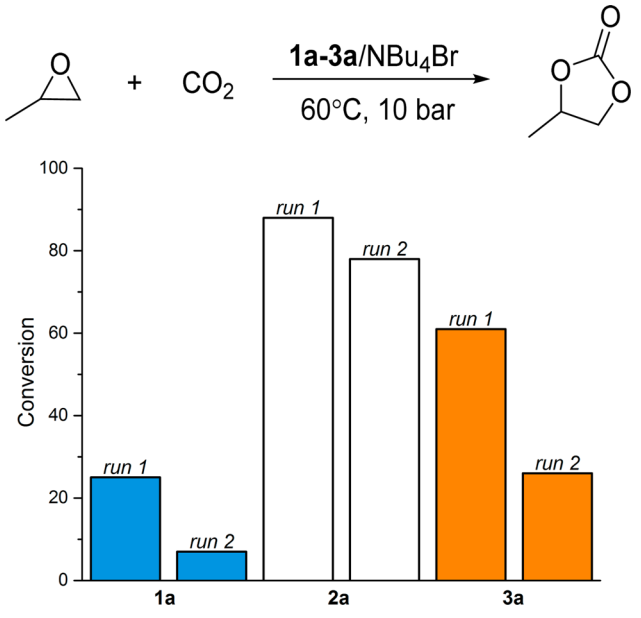

Figure 7. Top: Catalytic cycloaddition of CO_2 to propylene oxide (7 mL, 100 mmol) under mild conditions (60 °C, 10 bar, 18 h) using **1a** (1.1 g; 0.33 mmol of Nb), **2a** (0.5 g; 0.33 mmol of Nb) or **3a** (0.7 g; 0.33 mmol Nb) in the presence of NBu_4Br (1 mmol). For run 2, the recovered silica materials (ca. 95% of the initial amounts) were reused in the presence of 1 mmol NBu_4Br. Bottom: Conversion determined for catalysts **1a**−**3a** after two consecutive runs using fresh (left bar) and recycled (right bar) catalyst.

reaction as a catalyst. In all cases a reduction in catalytic efficiency was confirmed for each second run, however, **2a** exhibited the smallest reduction in catalytic conversion efficiency (90% to 81%), while **1a** and **3a** saw their conversions reduced dramatically to 7% and 26%, respectively. The loss of catalytic activity observed may be due, in part, to small amounts of the $NbCl_5{\cdot}OEt_2$ precursor remaining physisorbed on the silica surface after catalyst preparation that can actively participate in the first catalytic run as a homogeneous catalyst. However, it remains in the carbonate product once the reaction is completed, thus being removed after the first run (see Figure 7).

Therefore, considering the second run for assessing the activity of the supported catalysts, it appears that **2a** offers 3 times better performance than **3a** and 10 times better performance than **1a**. The reusability of the catalyst was investigated upon recovering the solid after each run. Accurate determination of the amount of Nb lost by **2a** through a number of catalytic cycles (see SI, Figure S10, and discussion on metal leaching experiments therein) proved the contribution of leached homogeneous $NbCl_5$ to be a negligible component in determining the catalytic activity of **2a**. The latter catalyst could be used for four catalytic cycles, although its catalytic activity progressively reduced to about one-third of the initial value. Elemental analysis data of **2a** recovered after four catalytic runs show that the progressive loss of catalytic activity is only partly due to the leaching of Nb as, at this point, nearly 70% of the initial amount of Nb can be found on the solid support. It is rather due to an alteration of the coordination sphere of the metal; the chlorine ligands are nearly completely depleted after four catalytic cycles (the Cl/Nb molar ratio in a sample of **2a** recovered after four cycles changed from 3.08 to just 0.1; see the SI for details), thus suppressing the acidity of the Nb center.

The difference in activity between the apparently similar heterogeneous Nb-based catalysts (**1a** and **2a** are both mostly monopodal species according to the ^{31}P and ^{93}Nb SSNMR experiments and DFT calculations, *vide supra*) can be tentatively explained in terms of the fine structure of the surface complexes. Interestingly, the catalytic activity **2a** > **3a** > **1a** determined experimentally follows the same order as that of the density of Nb atoms per unit area of surface (Table 1, considering the Nb loading per gram of silica). In particular, **2a** presents the highest density of $[\equiv SiONbCl_4{\cdot}OEt_2]$ surface species, and according to the double-quantum/single-quantum ^{31}P NMR correlation experiment carried out on **2b** (Figure 4), some of the niobium centers are proximate to one another on the surface. **3a** presents a lower density of surface Nb complexes (due to the formation of mostly bipodal surface complexes), and **1a**, given the high degree of dehydroxylation of the $SiO_{2\text{-}700}$ support, presents only completely isolated monopodal Nb surface complexes. The low catalytic activity measured for **1a** shows that the isolated $NbCl_5$ supported on silica is a poor catalyst under the mild reaction conditions employed. **2a**, on the other hand, presents neighboring Nb centers that might act in a cooperative fashion, comparably to the two centers of a bimetallic catalyst,[29] with the surface maintaining the niobium centers in close proximity. The beneficial effect of cooperating metal centers on the catalytic efficiency in the cycloaddition of CO_2 and epoxides has been demonstrated in the case of a bimetallic Al-salen catalyst. It has been attributed to the bifunctional role of the metal centers in the parallel activation of CO_2, via the formation of a hemicarbonate moiety, and of activation of the epoxide ring for the nucleophilic opening by a cocatalyst at the second metal center.[30] For the closely related reaction of CO_2/cyclohexene oxide copolymerization, cooperative catalysis between two zinc centers of homogeneous β-diiminate complexes has been reported by Moore et al.; in that case one Zn center is supposed to coordinate and activate the epoxide while the other Zn atom delivers the propagating polymer chain.[31] Indeed bimetallic catalysts are well established for this process.[32] Cooperative effects by metal centers of a bimetallic Co-catalyst have been observed as well for the enantioselective polymerization of epoxides.[33] In a recent study on the mechanism of the $NbCl_5$ catalyzed cycloaddition of CO_2 to PO in the homogeneous phase, D'Elia et al. have shown that the interaction between two Nb complexes might be required to lower the barrier for the insertion of CO_2 in the sterically hindered Nb−O bond generated on the hexacoordinated niobium center after the ring-opening of the epoxide.[3] In the transition state relative to the process of CO_2 insertion the Nb−Nb distance between the cooperating complexes was calculated to be 6.34 Å. On the surface, a bimetallic mechanistic proposal would require the existence of closely related niobium chloride species able to establish a cooperative interaction between two metal centers during the catalytic event. This would explain the experimental results displaying much higher catalytic activity for **2a** rather than **3a** or **1a**. To provide a mechanistic framework consistent with the experimental results of activation of CO_2 on the silica surface and to verify the possibility of an interaction between neighboring Nb centers during catalysis, mechanistic DFT calculations were undertaken.

Mechanistic DFT Calculations. Similarly to what was disclosed earlier during the discussion of the ^{93}Nb SSNMR parameters, to better reflect the experimental conditions in the

DOI: 10.1021/jacs.5b02872
J. Am. Chem. Soc. 2015, 137, 7728−7739

molecular-level calculations, two different silica cluster models have been applied. The first model is a silica cluster presenting a single silanol group (model 1), which we considered for monopodal, isolated species **1a** and contains a total of 31 atoms. The second model is a silica cluster presenting six silanol groups (model 2), which we considered for species **2a** and **3a** and contains a total of 78 atoms (Figure 8; see also the Experimental Section).[34] The energies computed for species **1a**–**3a** grafted on different sites of these silica models and under the different possible conformations are listed in Table 2,

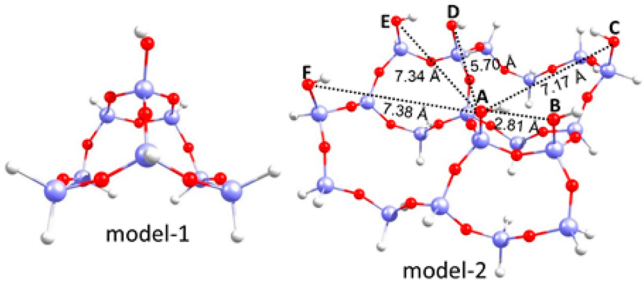

Figure 8. Optimized structures of the silica models considered in the present mechanistic DFT study. Color code: white, H; red, O; blue, Si.

Table 2. Computed Gibbs Free Energies (kcal/mol) of Grafting of Surface Species 1a, 2a, and 3a on Different Sites of Models 1 and 2

entry	species	site/model	*cis*[a] geometry	*trans*[a] geometry
1	**1a**	model 1	−5.4	−5.8
2		**A**/model 2	−10.2	−10.2
3	**2a**	**AB**/model 2	−20.6	−20.9
4		**AC**/model 2	−20.0	−23.2
5		**AD**/model 2	−16.0	−15.8
6		**AE**/model 2	−18.8	−19.0
7		**AF**/model 2	−17.9	−14.9
8	**3a**	**AB**	−8.5	−9.7
9		**AD**	11.5	10.5

[a]For entries 3–7, the geometry of [≡SiONbCl$_4$·OEt$_2$] at the **A** site is *trans*.

considering that NbCl$_5$·OEt$_2$ might graft on the surface in a "*cis*" or "*trans*" geometry (see also Figures S11–S13).

*Isolated Monopodal Species (**1a**).* The grafting of an isolated NbCl$_5$·OEt$_2$ on silica model 1 (**1a**) or model 2, with the release of an HCl molecule, is calculated to be a thermodynamically favorable process by 5.8 kcal/mol for model 1 and 10.2 kcal/mol for model 2, respectively (see Table 2, entries 1 and 2). Bearing in mind the structural difference between the silica models 1 and 2, we found that the different stability of species **1a** is due to the difference in the dispersion energy for the considered two models. For **1a**, the -OEt$_2$ group is preferentially *trans* oriented with respect to the O atom of the surface silanol (**1a**$_{trans}$, Figure S11b). The geometry of the *cis*-oriented species (**1a**$_{cis}$, Figure S11a) is calculated to be only 0.4 kcal/mol higher in energy, indicating that both species can be present under catalytic conditions.

For a monopodal species on model 2, the *trans* and *cis* isomers are isoenergetic. For the sake of simplicity, we considered species **1a**$_{trans}$ on model 1 to study the reaction mechanism for the cycloaddition of PO and CO$_2$ on an isolated Nb center on the silica surface.

*Neighboring Monopodal Species (**2a**).* For species **2a**, we explored all the possible grafting sites with one [≡SiONbCl$_4$·OEt$_2$] moiety grafted on the silanol labeled as **A**, at the center of the cluster of model 2 (Figure 8), and the other [≡SiONbCl$_4$·OEt$_2$] centers grafted alternatively on one of the neighboring silanol sites **B**–**F**, thus generating the model pairs labeled as **AB**, **AC**, **AD**, **AE**, and **AF** (or generically **AX**). We considered the -OEt$_2$ group of the Nb species grafted on site **A** in the *trans* configuration with respect to the surface silanol and explored both *cis* (**AX2a**$_{cis}$) and *trans* (**AX2a**$_{trans}$) configurations of the -OEt$_2$ group for the second Nb species placed at **B**–**F**. Based on the values reported in Table 2 for the **AB**–**AF** pairs (entries 3–7), the grafting of the second NbCl$_5$·OEt$_2$ molecule, in the presence of a [≡SiONbCl$_4$·OEt$_2$] moiety at site **A**, is thermodynamically favorable at all sites (in particular at the **AC** pair for the **AC2a**$_{trans}$ species with the release of an additional 13.0 kcal/mol) indicating that no steric repulsion originates from the grafting of a second NbCl$_5$·OEt$_2$ complex on neighboring silanols. This is true also for the closely related **AB** pair that can also generate a bipodal species (*vide infra*) and supports the observation that by adding an excess of NbCl$_5$·OEt$_2$ the grafting might produce a complete coverage of neighboring monopodal species as obtained in **2a**. A comparison between the *cis* and *trans* orientation of the OEt$_2$ groups relative to the surface shows that for the **AB**, **AD**, and **AE** pairs, the two geometries **2a**$_{cis}$ and **2a**$_{trans}$ are nearly isoenergetic. However, for the **AC** pair, the **AC2a**$_{trans}$ species is more thermodynamically favorable by ∼3.0 kcal/mol over its *cis* analogue, while this trend is opposite for the **AF** pair, i.e., **AF2a**$_{cis}$ is ∼3.0 kcal/mol more stable than the *trans* species.

The structure of model 2 offers the possibility to study the mechanism of the cycloaddition reaction of PO and CO$_2$ by exploring the interaction of neighboring [≡SiONbCl$_4$·OEt$_2$] species placed at different distances. The distance (measured at the anchoring O atoms) of the **AX** pairs ranges from 2.81 Å for **AB** to 7.17–7.38 Å of the **AC**, **AE**, and **AF** pairs.

For our mechanistic study we considered the **AX2a**$_{cis}$ species at sites **X** = **B**, **D**, and **F** (the latter was chosen as representative for all **AX** pairs having an O–O distance in the 7.17–7.38 range), having the surface silanol O–O distances at 2.81, 5.70, and 7.38 Å, respectively. The *cis* geometry was chosen as it is slightly more stable than the corresponding *trans* geometry for sites **D** and **F** (Table 2, entries 5–7), or nearly isoenergetic for site **B** (Table 2, entry 3). The optimized structures for the neighboring monopodal species used for the mechanistic investigation are reported in Figure S12.

*Bipodal Species (**3a**).* For species **3a**, the possible grafting sites on the silica model 2 are **AB** and **AD**, having the surface silanol O–O distances of 2.81 and 5.70 Å, respectively. Our results show that the bipodal grafting of NbCl$_5$·OEt$_2$ on the **AB** sites (**AB3a**$_{trans}$; see Figure S13a), with release of two HCl molecules, is favored by 9.7 kcal/mol (see Table 2, entry 8). Considering that monopodal NbCl$_5$·OEt$_2$ grafting at the **A** site leads to the release of 10.2 kcal/mol, this implies that the second grafting event is basically thermoneutral, indicating that the electronic gain due to the formation of the SiO-Nb bond is balanced by the strain energy. While the bipodal grafting of NbCl$_5$·OEt$_2$ on the **AB** pair sites is possible, bipodal grafting at the **AD** sites is endothermic by 10.5 kcal/mol (or ∼20.0 kcal/mol less favorable than the grafting at the **AB** sites),

DOI: 10.1021/jacs.5b02872
J. Am. Chem. Soc. 2015, 137, 7728–7739

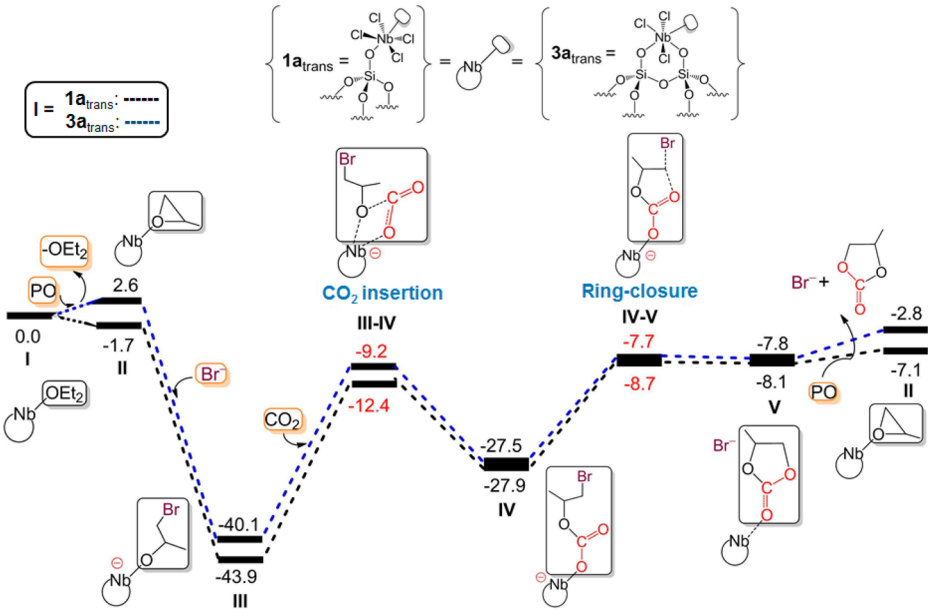

Figure 9. Computed free energy surface for the cycloaddition of propylene oxide (PO) and CO_2 catalyzed by species $\mathbf{1a}_{trans}$/NBu_4Br (black dashed lines) and species $\mathbf{3a}_{trans}$($\mathbf{AB3a}_{trans}$)/NBu_4Br (blue dashed lines). The free energies in solution (PO as the solvent) are given in kcal/mol relative to starting reactant species $\mathbf{1a}_{trans}$ and $\mathbf{3a}_{trans}$. The energy values in red represent the energies of the transition states.

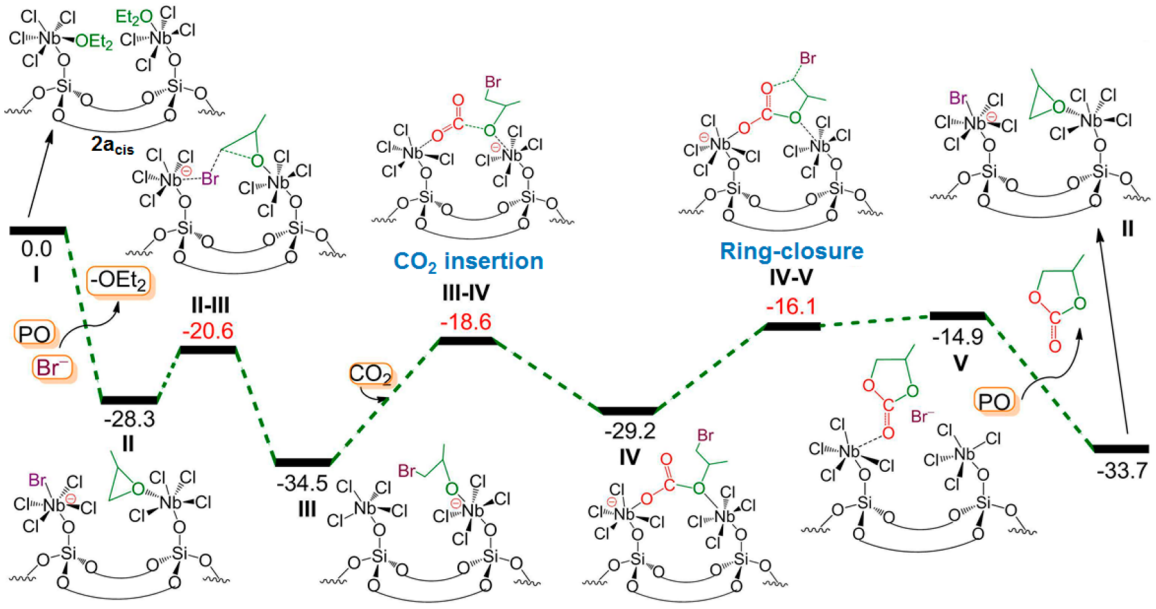

Figure 10. Computed free energy surface for the cycloaddition of propylene oxide (PO) and CO_2 catalyzed by species $\mathbf{2a}_{cis}$/NBu_4Br. The free energies in solution (PO as the solvent) are given in kcal/mol relative to starting reactant species $\mathbf{2a}_{cis}$. The energy values in red represent the energies of the transition states.

which indicates that for surface O−O distances as large as 5 Å the bipodal grafting would not occur. Site **AB** represents, therefore, the locations where a pair of monopodal Nb centers or a single bipodal species might be found according to the preparative conditions. Additionally, we explored the stability of the $\mathbf{AB3a}_{cis}$ species (see Figure S13b), and the resulting species was less thermodynamically stable (~1.0 kcal/mol) than $\mathbf{AB3a}_{trans}$. We considered the $\mathbf{AB3a}_{trans}$ species for the study of the reaction mechanism via a bipodal species.

*Reaction Pathways and Free Energy Surfaces for Model Surface Species Modeling Catalysts **1a**, **2a**, and **3a**.* Figures 9 and 10 show the most stable species and the free energy profiles for the cycloaddition of CO_2 to PO mediated by model silica supported compounds resembling catalyst **1a**−**3a**, in the presence of NBu_4Br as a source of bromide ions. In case of $\mathbf{1a}_{trans}$ and $\mathbf{3a}_{trans}$ ($\mathbf{AB3a}_{trans}$), the reaction pathway starts with the displacement of the OEt_2 ligand by a solvent PO molecule at the Nb of catalytic species **I** leading to the formation of intermediates **II** (Figure 9). For $\mathbf{2a}_{cis}$ ($\mathbf{AB2a}_{cis}$, $\mathbf{AD2a}_{cis}$, $\mathbf{AF2a}_{cis}$; for simplicity only the values corresponding to $\mathbf{AF2a}_{cis}$ are displayed), the two OEt_2 ligands are displaced by a PO molecule and a Br^- ion (Figure 10). Substitution of -OEt_2 by a PO on the Nb center is predicted to be thermodynamically favored by 1.7 kcal/mol for $\mathbf{1a}_{trans}$ and endergonic by

DOI: 10.1021/jacs.5b02872
J. Am. Chem. Soc. 2015, 137, 7728−7739

2.6 kcal/mol for $\mathbf{3a}_{trans}$, while the combined substitution of the OEt_2 by a PO on one Nb center, and by a bromide anion on the second Nb center in $\mathbf{AF2a}_{cis}$, is predicted to be highly exergonic with the release of 28.3 kcal/mol. The next step corresponds to the PO ring-opening of intermediates **II** by a Br anion, leading to the formation of more stable coordination intermediates **III**. For catalytic species $\mathbf{1a}_{trans}$ and $\mathbf{3a}_{trans}$, this step is predicted to be barrierless, which is in line with our previous results for the same process, but under homogeneous reaction conditions.[3] On the other hand, for species $\mathbf{AF2a}_{cis}$, the PO ring-opening barrier assisted by a Br^- ion is calculated to be just 7.7 kcal/mol above **II**. From a thermodynamic standpoint, for species $\mathbf{1a}_{trans}$ and $\mathbf{3a}_{trans}$, intermediate **III** lies 42.2 and 42.7 kcal/mol below the corresponding intermediate **II** and Br^-, respectively. For species $\mathbf{AF2a}_{cis}$, intermediate **III** lies 6.2 kcal/mol below **II**. The attack of the Br anion coordinated on a Nb center to the epoxide coordinated on a neighboring Nb atom as observed in $\mathbf{AF2a}_{cis}$ is reminiscent of the mechanism of epoxide ring-opening for the bimetallic Co-catalyst reported by Ahmed et al.[33b] In the next step we studied the insertion of CO_2 to give the hemicarbonate intermediate **IV**. For the case of $\mathbf{AF2a}_{cis}$, consistent with the mechanism proposed for the homogeneous catalysis,[3] where the CO_2 insertion step was assisted by a Nb center presenting a coordination vacancy, we considered intermediate **III** having a pentacoordinated Nb center. This presents a free coordination site next to the Nb center where CO_2 insertion takes place following the ring-opening by the Br anion. Our results show that the CO_2 insertion step is predicted to be the rate-determining step for all species studied. For instance, the predicted transition-state barrier **TS-III-IV** for $\mathbf{1a}_{trans}$ and $\mathbf{3a}_{trans}$ lies ~31.0 kcal/mol above **III**, while for $\mathbf{AF2a}_{cis}$, this barrier is reduced to 15.9 kcal/mol by considering the contribution of the neighboring Nb center. This observation is in line with the experiments, suggesting that the presence of a second Nb center bearing a vacant coordination site in proximity to the first Nb center is necessary to explain the higher catalytic activity of catalyst **2a** over **1a** and **3a**. Nevertheless, when considering the experimental temperature of 60 °C, the predicted barriers for $\mathbf{1a}_{trans}$ and $\mathbf{3a}_{trans}$ (~31.0 kcal/mol) are still reasonable as experimentally observed suggesting that the studied cycloaddition reaction might occur, albeit with much slower rate when compared with species $\mathbf{2a}_{cis}$. The predicted **TS-III-IV** barrier for $\mathbf{2a}_{cis}$ species on the **AD** pair sites (15.3 kcal/mol, see Figure S14) is similar to that calculated for the **AF** pair sites. Ring-opening on this site proceeds with a low barrier (3.1 kcal/mol) suggesting that on the selected silica model 2 all the possible sites containing $\mathbf{AX2a}_{cis}$ species with surface silanol O−O distances between 5.70 and 7.38 Å might have similar catalytic efficiency in terms of CO_2 insertion. In the case of sites **AB**, ring-opening of the epoxide (27.2 kcal/mol) and CO_2 insertion (28.8 kcal/mol) were found to occur with considerably higher barriers than for **AF** and **AD**. The higher values of these barriers arise from the lower degree of flexibility of the cooperating surface complexes due to the proximity of the corresponding surface oxygen atoms on **II** and **III**. However, the barrier calculated can be overcome at 60 °C. From **IV**, we studied the ring closing step to form the desired cyclic carbonate product **V**.

The predicted ring-closing barrier **TS-IV-V** for species $\mathbf{1a}_{trans}$ and $\mathbf{3a}_{trans}$ amounts to ~20.0 kcal/mol, while for species $\mathbf{AF2a}_{cis}$ this barrier is reduced to 13.1 kcal/mol (13.6 kcal/mol for $\mathbf{AD2a}_{cis}$). This observation indicates that the presence of a second Nb center may also contribute to reduce the cyclization barrier. For species $\mathbf{1a}_{trans}$ and $\mathbf{3a}_{trans}$, product **V** lies 8.1 and 7.8 kcal/mol below the starting species **I**, respectively, while for $\mathbf{AF2a}_{cis}$, product **V** is more stable being located 14.9 kcal/mol below **I**. Thus, the overall reaction energy profile is more exergonic in the case of species **2a** when compared with species **1a** and **3a**. Finally, intermediate **V** would release the carbonate product and a Br^- ion, regenerating the intermediate **II** with recoordination of a free PO molecule, in the case of species $\mathbf{1a}_{trans}$ and $\mathbf{3a}_{trans}$, and of both PO and a Br^- ion, in the case of species $\mathbf{AF2a}_{cis}$ thus closing the catalytic cycle. Based on these results, the experimentally observed higher catalytic activity of species **2a** over species **1a** and **3a** can be explained by the interaction between neighboring Nb centers that facilitates the steps of CO_2 insertion and ring closure by significantly reducing the corresponding barriers, **TS-III-IV** and **TS-IV-V**. The results presented for the mechanism of the heterogeneous catalytic reaction are in line with our proposed homogeneous catalytic mechanism for the same reaction.[3]

■ CONCLUSION

We have reported the preparation and the characterization of new surface complexes **1a**−**3a** and **1b**−**3b** obtained by grafting $NbCl_5{\cdot}OEt_2$ on $SiO_{2\text{-}700}$ (**1a**) and on $SiO_{2\text{-}200}$ (**2a**, **3a**) and by subsequent displacement of diethyl ether by PMe_3. **1a** and **1b** have been identified as monopodal niobium chloride species that are highly dispersed on silica dehydroxylated at 700 °C. Based on our combined SSNMR/DFT investigation, **2a**, **2b** and **3a**, **3b** have been shown to include monopodal and bipodal Nb complexes, with the population distributions depending on the amount of niobium precursor employed within the grafting protocol. **1a**−**3a** were employed as catalysts for the cycloaddition of propylene oxide and CO_2. Species **2a**, in which, according to our investigation, the Nb centers are placed in close proximity, has emerged as the most effective catalyst for this process. This spectacular effect has been correlated to the cooperative interaction between two Nb centers during the catalytic cycle, as supported by a systematic DFT investigation on model silica-supported niobium complexes. The mechanism developed for the heterogeneous process could be anticipated on the basis of our recent discoveries in the field of CO_2 activation by cooperating metal atoms.[3]

■ EXPERIMENTAL SECTION

Detailed descriptions of catalysis results and SSNMR experiments are provided in the Supporting Information.

Quantum Chemical Calculations of NMR Tensor Parameters. These quantum chemical computations were performed using the Amsterdam Density Functional (ADF) software, version 2010.02,[35] which is produced and distributed by Scientific Computing & Modelling (SCM). For geometry optimizations and NMR tensor calculations, the zeroth-order regular approximation (ZORA)[36] was used to include relativistic effects. Geometry optimizations included effects at the scalar level, while NMR tensor calculations included both scalar and spin−orbit contributions.[37] Calculations generally used an all-electron triple-ζ basis set which included polarization functions (i.e., TZ2P) and the generalized gradient approximation (GGA) exchange-correlation functional developed by Perdew, Burke, and Ernzerhof (i.e., PBE).[38] For the bipodal Nb species supported on silica, as a larger model of the silica surface was required, geometry optimizations used a partially frozen core basis to enhance computational efficiency. All computations included a dispersion correction, as specified by Grimme's three parameter model.[39] Magnetic shielding calculations were carried out using the "NMR" module which comes bundled with the ADF software.

DOI: 10.1021/jacs.5b02872
J. Am. Chem. Soc. 2015, 137, 7728−7739

For models of monopodal species on $SiO_{2\text{-}700}$, the initial silica surface selected for NMR property computations was taken from the previously optimized structure of Emsley and co-workers.[40] The surface species was exchanged from that of the prior study with the species of interest here and truncated at the second coordination sphere for the NMR tensor computations. Where applicable, oxygen atoms at the silica surface were terminated with hydrogen atoms. For all monopodal surfaces, the silicon and oxygen atoms at the surface were frozen, while the surface species of interest and the hydrogen atoms terminating the silica surface were optimized. Further details are provided in the SI (computational details and Tables S3 and S4).

Models of bipodal species on $SiO_{2\text{-}200}$ were constructed with the silica surface model of Sautet and co-workers.[34] The surface corresponds to a slice along the [001] plane of β-cristobalite which was found to be a stable phase of silica under the approximate conditions of the material under study (i.e., 200 °C and near ambient pressures). Taking the structure proposed by the authors (**001-4** in the original manuscript), a small cluster was selected and terminated with hydrogen atoms at all but two central positions. For these two positions, the surface species was anchored. All framework atoms, excepting the directly bound oxygen atoms, were held fixed, while the molecule on the surface was subjected to a geometry optimization.

For the molecular $NbCl_5$ species, atomic coordinates for one $(NbCl_5)_2$ dimer were taken from the original structure described by Cotton et al.[41] Due to the small size of this cluster, we were able to employ the large quadruple-ζ basis set (QZ4P) included within the ADF software package for NMR tensor calculations and did not include dispersion corrections. Other than these changes, computations were carried out in a similar fashion as compared to the surface-supported species. Euler angles were determined using EFGShield 4.1.[42] The coordinates for all the optimized structures, as well as the calculated bond energies can be found in Table S4.

Mechanistic Studies. All the DFT geometry optimizations were performed at the GGA BP86 level[43] with the Gaussian09 package.[44] The electronic configuration of the systems was described with the split-valence SVP basis set[45] for the main group atoms, while for Nb we adopted the quasi-relativistic SDD effective core potential, with the associated triple-ζ valence basis set.[46] The reported free energies were built through single point energy calculations on the BP86/SVP geometries using the BP86 functional and the triple-ζ TZVP[47] basis set on main group atoms, and the D3 version of Grimme's dispersion (empiricaldispersion=gd3).[39] Solvent effects were included with the PCM model using the modeled PO solvent. To these BP86/TZVP electronic energies in solvent, zero point energy, and thermal corrections were included from the gas-phase frequency calculations at the BP86/SVP level at T = 333.15 K and p = 1354 atm, as suggested by Martin et al.[48] The silica models in Figure 8 were elaborated from the work of Sautet et al.[34] using structure **001-5** for model 1 and structure **001-4** for model 2.

■ ASSOCIATED CONTENT

Ⓢ Supporting Information

General information, experimental procedures, IR and NMR spectra, additional catalytic results, leaching experiments, optimized structures for the silica supported complexes, and complete computational details. The Supporting Information is available free of charge on the ACS Publications website at DOI: 10.1021/jacs.5b02872.

■ AUTHOR INFORMATION

Corresponding Authors

*jeremie.pelletier@kaust.edu.sa
*jeanmarie.basset@kaust.edu.sa

Author Contributions

§V.D'E. and H.D. contributed equally.

Notes

The authors declare no competing financial interest.

■ ACKNOWLEDGMENTS

This work was supported by funds from King Abdullah University of Science and Technology and Saudi Basic Industries Corporation (SABIC). C.M.W. acknowledges the Natural Sciences and Engineering Council of Canada (NSERC) for a postdoctoral fellowship. Computational resources for selected DFT calculations were provided by the Pôle Scientifique de Modélisation Numérique (PSMN). J.D.A.P. and V.D'E. thank Alexander Barthel for his contribution.

■ REFERENCES

(1) (a) Tanabe, K. *Catal. Today* **2003**, *78*, 65. (b) Nery, M. S.; Ribeiro, R. P.; Lopes, C. C.; Lopes, R. S. C. *Synthesis* **2003**, 272. (c) Gallo, J. M. R.; Teixeira, S.; Schuchardt, U. *Appl. Catal. A-Gen.* **2006**, *311*, 199. (d) da Silva, L. C.; Lacerda, V.; Constantino, M. G.; da Silva, G. V. J. *Synthesis* **2008**, 2527. (e) Majhi, A.; Kim, S. S.; Kim, H. S. *Appl. Organomet. Chem.* **2008**, *22*, 466. (f) Fleming, F. F.; Ravikumar, P. C.; Yao, L. H. *Synlett* **2009**, 1077. (g) Gao, S. T.; Zhao, Y.; Li, C.; Ma, J. J.; Wang, C. *Synth. Commun.* **2009**, *39*, 2221. (h) Ravikumar, P. C.; Yao, L. H.; Fleming, F. F. *J. Org. Chem.* **2009**, *74*, 7294. (i) Yadav, J. S.; Reddy, B. V. S.; Reddy, A. S.; Reddy, C. S.; Raju, S. S. *Tetrahedron Lett.* **2009**, *50*, 6631. (j) Marchetti, F.; Pampaloni, G.; Patil, Y.; Galletti, A. M. R.; Hayatifar, M. *Polym. Int.* **2011**, *60*, 1722.

(2) (a) Monassier, A.; D'Elia, V.; Cokoja, M.; Dong, H. L.; Pelletier, J. D. A.; Basset, J. M.; Kuhn, F. E. *ChemCatChem* **2013**, *5*, 1321. (b) Dutta, B.; Sofack-Kreutzer, J.; Ghani, A. A.; D'Elia, V.; Pelletier, J. D. A.; Cokoja, M.; Kuhn, F. E.; Basset, J.-M. *Catal. Sci. Technol.* **2014**, *4*, 1534. (c) Wilhelm, M. E.; Anthofer, M. H.; Reich, R. M.; D'Elia, V.; Basset, J.-M.; Herrmann, W. A.; Cokoja, M.; Kuhn, F. E. *Catal. Sci. Technol.* **2014**, *4*, 1638.

(3) D'Elia, V.; Ghani, A. A.; Monassier, A.; Sofack-Kreutzer, J.; Pelletier, J. D. A.; Drees, M.; Vummaleti, S. V. C.; Poater, A.; Cavallo, L.; Cokoja, M.; Basset, J.-M.; Kühn, F. E. *Chem.—Eur. J.* **2014**, *20*, 11870−11882.

(4) Popoff, N.; Espinas, J.; Pelletier, J.; Macqueron, B.; Szeto, K. C.; Boyron, O.; Boisson, C.; Del Rosal, I.; Maron, L.; De Mallmann, A.; Gauvin, R. M.; Taoufik, M. *Chem.—Eur. J.* **2013**, *19*, 964.

(5) Chow, C.; Taoufik, M.; Quadrelli, E. A. *Eur. J. Inorg. Chem.* **2011**, 1349.

(6) Le Roux, E.; Taoufik, M.; Coperet, C.; de Mallmann, A.; Thivolle-Cazat, J.; Basset, J. M.; Maunders, B. M.; Sunley, G. J. *Angew. Chem., Int. Ed.* **2005**, *44*, 6755.

(7) Schrock, R. R.; Fellmann, J. D. *J. Am. Chem. Soc.* **1978**, *100*, 3359.

(8) (a) El Eter, M.; Hamzaoui, B.; Abou-Hamad, E.; Pelletier, J. D. A.; Basset, J. M. *Chem. Commun.* **2013**, *49*, 4616. (b) Espinas, J.; Pelletier, J. D. A.; Abou-Hamad, E.; Emsley, L.; Basset, J. M. *Organometallics* **2012**, *31*, 7610. (c) Popoff, N.; Espinas, J.; Pelletier, J.; Szeto, K. C.; Thivolle-Cazat, J.; Delevoye, L.; Gauvin, R. M.; Taoufik, M. *ChemCatChem* **2013**, *5*, 1971.

(9) Merle, N.; Trebosc, J.; Baudouin, A.; Del Rosal, I.; Maron, L.; Szeto, K.; Genelot, M.; Mortreux, A.; Taoufik, M.; Delevoye, L.; Gauvin, R. M. *J. Am. Chem. Soc.* **2012**, *134*, 9263.

(10) Mazoyer, E.; Trebosc, J.; Baudouin, A.; Boyron, O.; Pelletier, J.; Basset, J. M.; Vitorino, M. J.; Nicholas, C. P.; Gauvin, R. M.; Taoufik, M.; Delevoye, L. *Angew. Chem., Int. Ed.* **2010**, *49*, 9854.

(11) Szeto, K. C.; Loges, B.; Merle, N.; Popoff, N.; Quadrelli, A.; Jia, H. P.; Berrier, E.; De Mallmann, A.; Deleyoye, L.; Gauvin, R. M.; Taoufik, M. *Organometallics* **2013**, *32*, 6452.

(12) Johnston, K. E.; O'Keefe, C. A.; Gauvin, R. M.; Trebosc, J.; Delevoye, L.; Amoureux, J. P.; Popoff, N.; Taoufik, M.; Oudatchin, K.; Schurko, R. W. *Chem.—Eur. J.* **2013**, *19*, 12396.

(13) (a) Lo, A. Y. H.; Bitterwolf, T. E.; Macdonald, C. L. B.; Schurko, R. W. *J. Phys. Chem. A* **2005**, *109*, 7073. (b) de la Cruz, M. H. C.; Rocha, A. S.; Lachter, E. R.; Forrester, A. M. S.; Reis, M. C.; San Gil, R. A. S.; Caldarelli, S.; Farias, A. D.; Gonzalez, W. A. *Appl. Catal. A-Gen.* **2010**, *386*, 60. (c) Wang, X. F.; Smith, L. J. *J. Mol. Catal. A-Chem.* **2008**, *281*, 214. (d) Flambard, A.; Montagne, L.; Delevoye, L.; Palavit,

DOI: 10.1021/jacs.5b02872
J. Am. Chem. Soc. 2015, 137, 7728−7739

G.; Amoureux, J. P.; Videau, J. J. *J. Non-Cryst. Solids* **2004**, *345*, 75. (e) Lapina, O. B.; Khabibulin, D. F.; Shubin, A. A.; Terskikh, V. V. *Prog. Nucl. Magn. Reson. Spectrosc.* **2008**, *53*, 128. (f) Flambard, A.; Montagne, L.; Delevoye, L.; Steuernagel, S. *Solid State Nucl. Magn.* **2007**, *32*, 34. (g) Lapina, O. B.; Khabibulin, D. F.; Romanenko, K. V.; Gan, Z. H.; Zuev, M. G.; Krasil'nikov, V. N.; Fedorov, V. E. *Solid State Nucl. Magn.* **2005**, *28*, 204. (h) Zhou, D. H.; Hoatson, G. L.; Vold, R. L. *J. Magn. Reson.* **2004**, *167*, 242.

(14) (a) Cowley, A.; Fairbrother, F.; Scott, N. *J. Chem. Soc.* **1958**, 3133. (b) Fairbrother, F.; Cowley, A. H.; Scott, N. *J. Less-Common Met.* **1959**, *1*, 206.

(15) (a) Komer, W. D.; Machin, D. J. *J. Less-Common Met.* **1978**, *61*, 91. (b) Millot, N.; Santini, C. C.; Lefebvre, F.; Basset, J. M. *C.R. Chim.* **2004**, *7*, 725.

(16) Marchetti, F.; Pampaloni, G.; Zacchini, S. *Inorg. Chem.* **2008**, *47*, 365.

(17) Wieser, H.; Laidlaw, W. G.; Krueger, P. J.; Fuhrer, H. *Spectrochim. Acta* **1968**, *A 24*, 1055.

(18) Merbach, A. A.; Bunzli, J. C. *Helv. Chim. Acta* **1972**, *55*, 580.

(19) (a) Lesage, A.; Bardet, M.; Emsley, L. *J. Am. Chem. Soc.* **1999**, *121*, 10987. (b) Fayon, F.; Le Saout, G.; Emsley, L.; Massiot, D. *Chem. Commun.* **2002**, 1702. (c) Cadars, S.; Sein, J.; Duma, L.; Lesage, A.; Pham, T. N.; Baltisberger, J. H.; Brown, S. P.; Emsley, L. *J. Magn. Reson.* **2007**, *188*, 24.

(20) Harris, R. K.; Becker, E. D.; De Menezes, S. M. C.; Goodfellow, R.; Granger, P. *Pure Appl. Chem.* **2001**, *73*, 1795.

(21) Du, L. S.; Schurko, R. W.; Kim, N.; Grey, C. P. *J. Phys. Chem. A* **2002**, *106*, 7876.

(22) Schurko, R. W. *Acc. Chem. Res.* **2013**, *46*, 1985.

(23) Kemp, T. F.; Smith, M. E. *Solid State Nucl. Magn.* **2009**, *35*, 243.

(24) Samantaray, M. K.; Callens, E.; Abou-Hamad, E.; Rossini, A. J.; Widdifield, C. M.; Dey, R.; Emsley, L.; Basset, J. M. *J. Am. Chem. Soc.* **2014**, *136*, 1054.

(25) (a) Comerford, J. L.; Ingram, I. D. V.; North, M.; Wu, X. *Green Chem.* **2015**, *17*, 1966−1987. (b) Pescarmona, P. P.; Taherimehr, M. *Catal. Sci. Technol.* **2012**, *2*, 2169−2187. (c) Marin, C.; Fiorani, G.; Kleij, A. W. *Acs Catal.* **2015**, *5*, 1353−1370. (d) North, M.; Pasquale, R.; Young, C. *Green Chem.* **2010**, *12*, 1514−1539. (e) Laserna, V.; Fiorani, G.; Whiteoak, C. J.; Martin, E.; Escudero-Adan, E.; Kleij, A. W. *Angew. Chem., Int. Ed.* **2014**, *53*, 10416−10419. (f) Kim, S. H.; Hong, S. H. *Acs Catal.* **2014**, *4*, 3630−3636. (g) Beattie, C.; North, M.; Villuendas, P.; Young, C. *J. Org. Chem.* **2013**, *78*, 419−426.

(26) (a) Melendez, J.; North, M.; Villuendas, P.; Young, C. *Dalton Trans.* **2011**, *40*, 3885. (b) Melendez, J.; North, M.; Villuendas, P. *Chem. Commun.* **2009**, 2577−2579.

(27) (a) Song, J. L.; Zhang, Z. F.; Hu, S. Q.; Wu, T. B.; Jiang, T.; Han, B. X. *Green Chem.* **2009**, *11*, 1031. (b) Zalomaeva, O. V.; Chibiryaev, A. M.; Kovalenko, K. A.; Kholdeeva, O. A.; Balzhinimaev, B. S.; Fedin, V. P. *J. Catal.* **2013**, *298*, 179. (c) Guillerm, V.; Weseliński Ł, J.; Belmabkhout, Y.; Cairns, A. J.; D'Elia, V.; Wojtas, Ł.; Adil, K.; Eddaoudi, M. *Nat. Chem.* **2014**, *6*, 673. (d) Feng, D.; Chung, W.-C.; Wei, Z.; Gu, Z.-Y.; Jiang, H.-L.; Chen, Y. P.; Darensbourg, D. J.; Zhou, H. C. *J. Am. Chem. Soc.* **2013**, *135*, 17105. (e) Beyzavi, M. H.; Klet, R. C.; Tussupbayev, S.; Borycz, J.; Vermeulen, N. A.; Cramer, C. J.; Stoddart, J. F.; Hupp, J. T.; Farha, O. K. *J. Am. Chem. Soc.* **2014**, *136*, 15861.

(28) (a) Chun, J.; Kang, S.; Kang, N.; Lee, S. M.; Kim, H. J.; Son, S. U. *J. Mater. Chem. A* **2013**, *1*, 5517. (b) Xie, Y.; Wang, T. T.; Liu, X. H.; Zou, K.; Deng, W. Q. *Nat. Commun.* **2013**, *4*, No. 1960.

(29) (a) Haak, R. M.; Wezenberg, S. J.; Kleij, A. W. *Chem. Commun.* **2010**, *46*, 2713. (b) Shibasaki, M.; Yamamoto, Y. *Multimetallic Catalysts in Organic Synthesis*; Wiley-VCH Verlag GmbH & Co. KGaA: Weinheim, 2005.

(30) (a) Clegg, W.; Harrington, R. W.; North, M.; Pasquale, R. *Chem.—Eur. J.* **2010**, *16*, 6828. (b) North, M.; Pasquale, R. *Angew. Chem., Int. Ed.* **2009**, *48*, 2946.

(31) Moore, D. R.; Cheng, M.; Lobkovsky, E. B.; Coates, G. W. *J. Am. Chem. Soc.* **2003**, *125*, 11911−11924.

(32) (a) Kissling, S.; Lehenmeier, M. W.; Altenbuchner, P. T.; Kronast, A.; Reiter, M.; Deglmann, P.; Seemann, U. B.; Rieger, B. *Chem. Commun.* **2015**, *51*, 4579−4582. (b) Liu, Y.; Ren, W.-M.; Liu, C.; Fu, S.; Wang, M.; He, K.-K.; Li, R.-R.; Zhang, R.; Lu, X.-B. *Macromolecules* **2014**, *47*, 7775−7788. (c) Kember, M. R.; Williams, C. K. *J. Am. Chem. Soc.* **2012**, *134*, 15676−15679.

(33) (a) Ahmed, S. M.; Poater, A.; Childers, M. I.; Widger, P. C. B.; LaPointe, A. M.; Lobkovsky, E. B.; Coates, G. W.; Cavallo, L. *J. Am. Chem. Soc.* **2013**, *135*, 18901−18911. (b) Widger, P. C. B.; Ahmed, S. M.; Hirahata, W.; Thomas, R. M.; Lobkovsky, E. B.; Coates, G. W. *Chem. Commun.* **2010**, *46*, 2935−2937.

(34) Rozanska, X.; Delbecq, F.; Sautet, P. *Phys. Chem. Chem. Phys.* **2010**, *12*, 14930.

(35) (a) Guerra, C. F.; Snijders, J. G.; te Velde, G.; Baerends, E. J. *Theor. Chem. Acc.* **1998**, *99*, 391. (b) te Velde, G.; Bickelhaupt, F. M.; Baerends, E. J.; Guerra, C. F.; Van Gisbergen, S. J. A.; Snijders, J. G.; Ziegler, T. *J. Comput. Chem.* **2001**, *22*, 931.

(36) (a) van Lenthe, E.; Baerends, E. J.; Snijders, J. G. *J. Chem. Phys.* **1993**, *99*, 4597. (b) Vanleeuwen, R.; Baerends, E. J. *Int. J. Quantum Chem.* **1994**, *52*, 711. (c) van Lenthe, E.; Ehlers, A.; Baerends, E. J. *J. Chem. Phys.* **1999**, *110*, 8943.

(37) van Lenthe, E.; Snijders, J. G.; Baerends, E. J. *J. Chem. Phys.* **1996**, *105*, 6505.

(38) (a) Perdew, J. P.; Burke, K.; Ernzerhof, M. *Phys. Rev. Lett.* **1996**, *77*, 3865. (b) Perdew, J. P.; Burke, K.; Ernzerhof, M. *Phys. Rev. Lett.* **1997**, *78*, 1396.

(39) Grimme, S.; Antony, J.; Ehrlich, S.; Krieg, H. *J. Chem. Phys.* **2010**, *132*, 154104.

(40) Blanc, F.; Basset, J. M.; Coperet, C.; Sinha, A.; Tonzetich, Z. J.; Schrock, R. R.; Solans-Monfort, X.; Clot, E.; Eisenstein, O.; Lesage, A.; Emsley, L. *J. Am. Chem. Soc.* **2008**, *130*, 5886.

(41) Cotton, F. A.; Kibala, P. A.; Matusz, M.; Sandor, R. B. W. *Acta Crystallogr. C* **1991**, *47*, 2435.

(42) Adiga, S.; Aebi, D.; Bryce, D. L. *Can. J. Chem.* **2007**, *85*, 496.

(43) (a) Becke, A. D. *Phys. Rev. A* **1988**, *38*, 3098. (b) Perdew, J. P. *Phys. Rev. B* **1986**, *33*, 8822. (c) Perdew, J. P. *Phys. Rev. B* **1986**, *34*, 7406.

(44) Frisch, M. J.; Trucks, G. W.; Schlegel, H. B.; Scuseria, G. E.; Robb, M. A.; Cheeseman, J. R.; Scalmani, G.; Barone, V.; Mennucci, B.; Petersson, G. A.; Nakatsuji, H.; Caricato, M.; Li, X.; Hratchian, H. P.; Izmaylov, A. F.; Bloino, J.; Zheng, G.; Sonnenberg, J. L.; Hada, M.; Ehara, M.; Toyota, K.; Fukuda, R.; Hasegawa, J.; Ishida, M.; Nakajima, T.; Honda, Y.; Kitao, O.; Nakai, H.; Vreven, T.; Montgomery, J. A., Jr.; Peralta, J. E.; Ogliaro, F.; Bearpark, M.; Heyd, J. J.; Brothers, E.; Kudin, K. N.; Staroverov, V. N.; Kobayashi, R.; Normand, J.; Raghavachari, K.; Rendell, A.; Burant, J. C.; Iyengar, S. S.; Tomasi, J.; Cossi, M.; Rega, N.; Millam, N. J.; Klene, M.; Knox, J. E.; Cross, J. B.; Bakken, V.; Adamo, C.; Jaramillo, J.; Gomperts, R.; Stratmann, R. E.; Yazyev, O.; Austin, A. J.; Cammi, R.; Pomelli, C.; Ochterski, J. W.; Martin, R. L.; Morokuma, K.; Zakrzewski, V. G.; Voth, G. A.; Salvador, P.; Dannenberg, J. J.; Dapprich, S.; Daniels, A. D.; Farkas, Ö.; Foresman, J. B.; Ortiz, J. V.; Cioslowski, J.; Fox, D. J. *Gaussian 09*, Revision A.1; Gaussian, Inc.: Wallingford, CT, 2009.

(45) Schaefer, A.; Horn, H.; Ahlrichs, R. *J. Chem. Phys.* **1992**, *97*, 2571.

(46) (a) Haeusermann, U.; Dolg, M.; Stoll, H.; Preuss, H. *Mol. Phys.* **1993**, *78*, 1211. (b) Kuechle, W.; Dolg, M.; Stoll, H.; Preuss, H. *J. Chem. Phys.* **1994**, *100*, 7535. (c) Leininger, T.; Nicklass, A.; Stoll, H.; Dolg, M.; Schwerdtfeger, P. *J. Chem. Phys.* **1996**, *105*, 1052.

(47) Schaefer, A.; Huber, C.; Ahlrichs, R. *J. Chem. Phys.* **1994**, *100*, 5829.

(48) Martin, R. L.; Hay, P. J.; Pratt, L. R. *J. Phys. Chem. A* **1998**, *102*, 3565.

DOI: 10.1021/jacs.5b02872
J. Am. Chem. Soc. 2015, 137, 7728−7739